Birnavirus Ribonucleoprotein Assembly

Idoia Busnadiego[1,2,*], Maria T. Martín[3], Diego S. Ferrero[1,4], María G. Millán de la Blanca[1,5], Laura Broto[1], Elisabeth Díaz-Beneitez[1], Daniel Fuentes[1], Dolores Rodríguez[1], Nuria Verdaguer[4], Leonor Kremer[3] and José F. Rodríguez[1*]

(1) Departamento de Biología Molecular y Celular. Centro Nacional de Biotecnología, Madrid, 28049, Spain (2) Institute of Medical Virology, University of Zurich, Zurich, 8057, Switzerland. (3) Protein Tools Unit and Department of Immunology and Oncology. Centro Nacional de Biotecnología, Madrid, 28049, Spain (4) Departamento de Biologia Estructural. Institut de Biología Molecular de Barcelona, Barcelona, 08028, Spain (5) Departamento de Reproducción Animal. Instituto Nacional de Investigación y Tecnología Agraria y Alimentaria. Madrid, 28040, Spain.

* To whom correspondence should be addressed. Idoia Busnadiego. Tel: +41 44 63 42620; Email: busnadiego.idoia@virology.uzh.ch. Correspondence may also be addressed to José F. Rodríguez. Email: jfrodrig@cnb.cisc.es

ABSTRACT

Birnaviruses are ancient evolutionary intermediates between double- and single-stranded RNA viruses that package their dsRNA genomes as filamentous ribonucleoproteins (RNP). The major RNP protein component is VP3, a homodimeric polypeptide that functionally mimics nucleoproteins from single stranded RNA viruses. An experimentally-tested VP3-dsRNA interaction model underlying the assembly of Birnavirus RNPs. Our report provides new and relevant clues to better understanding the molecular biology of this unique virus family.

25 **INTRODUCTION**

26 Double-stranded (ds) RNA duplexes are ubiquitously found in all live entities.
27 dsRNA modules are indeed essential for a wide variety of biological processes, e.g.
28 mRNA splicing and transport, gene transcription and mRNA translation. The multiple
29 roles played by dsRNA modules entail their interaction with specific protein partners.
30 Ribosomes and spliceosomes are good examples of the importance of these interactions
31 for the maintenance of life. Paralleling their paramount biological significance, dsRNA-
32 protein interactions have been analysed using a wide variety of experimental
33 approaches, thus multiple dsRNA-binding proteins have been structurally characterized
34 leading to a better understanding on how proteins recognize and interact with RNA
35 duplexes (1,2).

36 Viruses, especially those harbouring dsRNA genomes, are utterly dependent
37 upon dsRNA-protein interactions both to successfully completing their replication
38 program and preventing detection by host-encoded dsRNA pattern recognition
39 receptors (PRRs) and dsRNA-dependent antiviral effectors that constitute a major
40 component of the cellular innate antiviral response (3).

41 The *Birnaviridae* family comprises a group of non-enveloped icosahedral viruses
42 harbouring bi-segmented, double-stranded RNA (dsRNA) genomes (4). Members of this
43 family infect insects, aquatic fauna and birds. Within this family, Drosophila X (DXV),
44 pancreatic necrosis (IPNV), blotched snakehead (BSV) and infectious bursal disease virus
45 (IBDV) are prototype members of the entomo-, aqua-, blosna- and avibirnavirus genera,
46 respectively (4).

47 IBDV, the best characterized member of this family, infects domestic chickens
48 (*Gallus gallus*) causing an acute immunosuppressive disease that imposes severe loses

49 to the poultry industry worldwide (5). The IBDV major structural components namely
50 VP2 (the capsid polypeptide) and VP3 (a multifunctional polypeptide), are encoded by
51 the polyprotein open reading frame (6). The polyprotein undergoes a co-translational,
52 self-proteolytic processing that releases pVP2 (the capsid polypeptide precursor) along
53 with VP4 (the viral protease) and VP3 (7). VP3 is multifunctional participating in several
54 processes during IBDV replication, i.e. acting as a scaffolding element during particle
55 morphogenesis (8,9,10), activating the virus-encoded RNA-dependent RNA polymerase
56 (RdRP, also known as VP1) (11,12), and interacting with both dsRNA genome segments
57 to form ribonucleoprotein (RNP) complexes that occupy the inner particle space (13).

58 Prototypical dsRNA viruses, e.g. members of the *Reoviridae* family, enclose their
59 multipartite genomes into a conserved icosahedral structure, known as transcriptional
60 core, which remains intact throughout the replication cycle. This structure holds the
61 enzymatic machinery required for genome replication, transcription and mRNA
62 extrusion whilst providing an efficient shelter against dsRNA host sensor proteins (14).
63 In a sharp structural and functional contrast, Birnaviruses lack replicative cores (15-17).
64 This structure is functionally replaced by RNP complexes built by the genome dsRNA
65 segments associated to VP3 dimers. The third, and minor, RNP component is the virus-
66 encoded RNA polymerase (VP1), which is found in two molecular forms, i.e. as a free
67 polypeptide and as VPg, covalently linked to the 5'-ends of both genome dsRNA
68 segments (18,19). RNPs are transcriptionally active, *in vitro* and *ex vivo*, and act as
69 transcriptional/replication devices capable of triggering a productive infection in the
70 absence of the capsid protein (19,20).

71 Like other dsRNA binding proteins, e.g. NS1 from influenza virus (21) and E3 from
72 vaccinia virus (VACV) (22), *in vitro* assays indicate that VP3 shields viral dsRNA from

73 cellular dsRNA sensors, thus preventing the activation of at least two major components
74 of the host's innate antiviral protein arsenal, namely the protein kinase RNA-activated
75 (PKR) (23) and the melanoma differentiation-associated protein 5 (MDA5) (24).
76 Additionally, we have also found that VP3 acts as an efficient anti-silencing protein in an
77 experimental virus/plant model (25).

78 According to our preliminary mapping, the VP3 polypeptide holds a bipartite
79 dsRNA binding domain (dsRBD) located at the central region of the protein (25). The
80 dsRBD encompasses two surface exposed electropositive regions, termed Patch1 and
81 Patch2, located at the same protein face. Each region holds four electropositive
82 residues: Patch1 (K99, R102, K105 and K106) and Patch2 (R159, R168, H198 and R200)
83 (25). The central VP3 region harbouring the dsRBD folds in two α-helical modules
84 connected by a long and flexible hinge and is organized as a swapped dimer (26).

85 So far, attempts to solving the crystal structure of VP3 bound to dsRNA have
86 failed, thus hindering the possibility of obtaining precise information about the VP3-
87 dsRNA interaction mechanism. Here, we present an *in silico* model docking the VP3
88 dimer on the A-form of the dsRNA helix. The model has been tested using surface
89 plasmon resonance (SPR) analysis performed with a collection of VP3 mutant versions
90 and RNA duplexes of different lengths. Experimental data are in good agreement with
91 the interaction model. We have also identified K99 and K106 as the critical residues for
92 dsRNA binding. Indeed, mutations affecting either one of these two residues abrogate
93 both the capacity of the protein to bind dsRNA and shield dsRNA from cellular sensors,
94 and thwart virus infectivity.

95 **MATERIALS AND METHODS**

96 **Cells and viruses**

97 BSC-1 (African green monkey kidney cells, ATCC number CRL-2761), DF-1 (spontaneously
98 transformed chicken embryo fibroblasts, ATCC number CRL-12203) and QM7 (quail
99 muscle myoblasts, ATCC number CRL-19DF cells were grown in Dulbecco's modified
100 minimal essential medium (DMEM). *HighFive* cells (*Trichoplusia ni* ovary cells, BTI-TN-
101 5B1-4, Invitrogen) were grown in TC-100 medium (Gibco). All cell media were
102 supplemented with penicillin (100 U/ml), streptomycin (100 µg/ml) and 10% fetal calf
103 serum (FCS) (Sigma-Aldrich, Spain). The recombinant VACV VT7LacOI, kindly provided by
104 B. Moss (National Institute of Health, Bethesda, Maryland, USA), was grown and titrated
105 in BSC-1 cells as previously described (27). All recombinant baculoviruses (rBV) used in
106 this report were grown and titrated in HighFive cells following instructions provided in
107 the Bac-to-Bac Baculovirus Expression System manual (Invitrogen, Publication Number
108 MAN0000414. Revision A.0.). IBDV infections and titrations were carried out in QM7
109 cells as previously described (28).

110 **Generation of rBVs**

111 rBVs FB/his-VP3, FB/his-VP3P1 and FB/his-VP3P2, used for the production of
112 recombinant hVP3, hVP3P1 and hVP3P2 have been described elsewhere (25,29). Other
113 rBVs used in this report were generated as follows. The construction of baculovirus
114 transfer vectors encoding hVP3 mutant polypeptides were generated using PCR-based
115 site directed mutagenesis on the pFB/hisVP3 plasmid (29) using synthetic DNA
116 oligonucleotide primers (Sigma-Aldrich) described in Supplemental Table 1. The
117 resulting plasmids, pFB/hVP3K99D, pFB/hisVP3R102D, pFB/hVP3K105D and
118 pFB/hVP3K106D, respectively, were used for the introduction of double mutations using

119 the corresponding oligonucleotide primers (Supplemental Table 1), thus generating
120 plasmids pFB/hVP3K99D-R102D, pFB/hVP3K99D-K105D, pFB/hVP3K99D-K106D,
121 pFB/hVP3R102D-K105D, pFB/hVP3R102D-K106D and pFB/hisK105D-K106D). Plasmids
122 were subjected to nucleotide sequencing and then used to generate rBVs using the Bac-
123 to-Bac system (Invitrogen, USA).

124 **Generation of pcDNA3-VP3 plasmids**

125 Generation of pcDNA3-VP3wt has been described elsewhere (23). For the
126 generation of pcDNA3VP3Patch1, pcDNA3VP3Patch2, pcDNA3VP3Patch1+2,
127 pcDNAVP3K99D, pcDNAVP3R102D, pcDNAVP3K105D and pcDNAVP3K106D, DNA
128 fragments corresponding to each of the VP3 coding regions were generated by PCR from
129 the previously described pFB baculovirus transfer vectors using the primers 5'-
130 CGCGAAGCTTATGGGTTTCCCTCACAATCCACGC and 5'-
131 GCGCGGATCCTCACTCAAGGTCCTCATCAGAGAC. The DNA fragments were purified,
132 restricted with HindIII and BamHI and cloned into pcDNA3 (Invitrogen) previously
133 digested with the same enzymes. The resulting plasmids were subjected to nucleotide
134 sequence analysis to assess the correctness of the cloned sequence.

135 **Generation of recombinant VACV expressing mutant versions of the VP3 polypeptide**

136 The production of recombinant VACV (rVACV) VT7/VP3K99D and
137 VT7/VP3K106D, was initiated by generating the corresponding VACV insertion vectors.
138 For this, two DNA fragments of 789 bp containing the VP3K99D and VP3K106D mutant
139 versions of the VP3 ORF, flanked by NdeI and BamHI restriction sites, were generated
140 by PCR using the plasmids pFB/hisVP3K99D and pFB/hisVP3K106D as templates and the
141 primers 5'GCGCCATATGGCTGCATCAGAGTTCAAAGAG and
142 5'GCGCGGATCCTCACTCAAGGTCCTCATCAGAG. The resulting PCR products were

143 purified, digested with NdeI and BamHI and ligated to the pVOTE.2 VACV
144 insertion/expression plasmid vector (27) previously digested with the same restriction
145 enzymes. The resulting plasmids, pVOTE/VP3K99D and pVOTE/VP3K106D, were
146 subjected to nucleotide sequencing, and then used to generate the corresponding
147 rVACVs, VT7/VP3K99D and VT7/VP3K106D, via homologous recombination with the VT7
148 VACV genome as previously described (27).

149 **Expression and Purification of his-tagged VP3 protein versions from Insect cells**

150 Expression of the different hVP3 protein versions was achieved by infecting
151 HighFive cell monolayers with the rBVs described above at a MOI of 3 PFU/cell. Infected
152 cells were harvested at 72 h post-infection (PI), washed twice with phosphate-buffered
153 saline, resuspended in lysis buffer (50 mM Tris-HCl [pH 8.0], 500 mM NaCl, 0.1% igepal)
154 supplemented with protease inhibitors (Complete Mini; Roche), and maintained on ice
155 for 20 min. Thereafter, extracts were centrifuged at 13,000xg for 10 min at 4°C.
156 Supernatants were collected and subjected to metal-affinity chromatography (IMAC)
157 purification by using a HisTrap HP Ni^{2+} affinity column (GE Healthcare, Spain). Resin-
158 bound polypeptides were released with elution buffer (50 mM Tris-HCl [pH 8.0], 500
159 mM NaCl, 250 mM imidazol). hisVP3-containing fractions were pooled, dialyzed against
160 lysis buffer lacking igepal, and subjected to a second purification round under identical
161 conditions. Finally, protein samples were dialyzed against 1,000 volumes of 50 mM Tris-
162 HCl (pH 8.0), 150 mM NaCl. The purity of eluted proteins was assessed by SDS-PAGE
163 analysis and Coomassie blue staining. Protein concentration was determined using the
164 BCA Protein Assay Kit (Thermo Scientific Pierce, USA). Purified proteins were maintained
165 at 4°C for a maximum period of 14 days.

166 **Generation of dsRNA analytes**

167 RNA duplex preparation was performed by annealing complementary synthetic
168 single stranded RNA oligonucleotide pairs where one of the oligonucleotides from each
169 pair was biotinylated at its 5'-end. Both oligonucleotide synthesis and annealing was
170 performed by the manufacturer (Biomers.net, Germany). Oligonucleotide sequences
171 are described in Supplemental Table 2.

172 **Surface Plasmon Resonance Analysis**

173 SPR experiments were performed using a biosensor Biacore 3000 (Biacore, GE
174 Healthcare). dsRNA ligands bearing a biotin at the 5`end of one the strands were
175 immobilized on the surface of streptavidin-coated sensor chips (SA). RNA duplexes were
176 loaded at a flow rate of 10 µl/min, using HBS-P (10 mM HEPES [pH 7.4], 0.2 M NaCl, 3
177 mM EDTA, 0.005% Surfactant P20) running buffer. Reference surfaces, used as control
178 for these assays, were blank flow cells.

179 Binding assays, performed in duplicate within each experiment, were carried out
180 at 25°C at a flow rate of 30 µl/min. Proteins under study were serially diluted in running
181 buffer to reach the indicated concentrations. The protein fraction that remained bound
182 after the dissociation phase was removed by injecting 800 mM NaCl. Data were collected
183 for the association and dissociation periods as indicated in each specific experiment. SPR
184 sensograms recorded with each tested protein concentration were overlaid, aligned and
185 analysed using the BIAevaluation Software 4.1 (GE Healthcare). All data sets were
186 processed using a double-referencing method (30). Collected data were fit to a 1:1
187 Langmuir model with a correction for mass transport (31).

188 **IBDV reverse genetics analysis**

189 The reverse genetics analysis was performed as previously described (32) using
190 an approach based on the co-transfection of QM7 cells with two plasmids containing

191 cDNAs corresponding to the positive strand sequence of the IBDV segments A and B,
192 respectively. Plasmid pT7-SA-Rz harboring the cDNA of segment A was subjected to site
193 directed mutagenesis to introduce mutations VP3K99D or VP3K106D within the context
194 of the IBDV polyprotein open reading frame. Mutagenesis was performed as described
195 above using primer pairs K99DFW and K99DREV or K106DFW and K106DREV
196 (Supplemental Table 1). The resulting plasmids, pT7-SAVP3K99D-Rz and pT7-
197 SAVP3K106D-Rz, were subjected to nucleotide sequence analysis to assess their
198 correctness.

199 QM7 cells were transfected with a combination of plasmids pT7-SA-Rz and pT7-
200 SB-Rz, corresponding to the IBDV wild-type genome segments, pT7-SAVP3K99D-Rz and
201 pT7-SB-Rz, or pT7-SAVP3K106D-Rz and pT7-SB-Rz, respectively, using Lipofectamine
202 2000 (Invitrogen). At 6 h post-transfection, cultures were infected with 3 PFU/cell of
203 VT7, an rVV inducibly expressing the T7 RNA polymerase. Cultures were then maintained
204 at 37°C in medium supplemented with 1 mM isopropyl-D-thiogalactosidase (IPTG). At
205 72 h PI, cultures were harvested and subjected to three freeze-thaw cycles. Infected cell
206 samples were used to assess the expression of the VP3 polypeptide by Western blotting.
207 After removing cell debris by low speed centrifugation, supernatants were recovered
208 and filtered through 0.1 µm filters (Merk Millipore) to eliminate contaminant rVV
209 particles, and used to infect fresh QM7 cell monolayers. Samples from these infections
210 were collected at 72 h PI and used to rule out possible contamination with the rVACV by
211 Western blotting by using the monoclonal antibody mAbC3 recognizing a highly
212 abundant VACV structural protein (33). The corresponding cell supernatants were used
213 to perform two subsequent rounds of IBDV amplification by infecting fresh QM7

214 monolayers. The presence of IBDV in all samples was assessed by plaque assay as
215 previously described (28).

216 **Characterization of IBDV virus-like particles in cells infected with rVACV**

217 BSC-1 cell monolayers were infected with rVACV VT7/VP3, VT7/VP3K99D or
218 VT7/VP3K106D at a MOI of 3 PFU/cell. Transmission electron microscopy (TEM) analysis
219 was performed using cell samples collected at 48 h PI following a previously described
220 protocol (9). Purification of IBDV virus-like particles (VLP) was carried out using samples
221 collected at 72 h PI as previously described (34). VLP samples were negatively stained
222 with 2% aqueous uranyl acetate. TEM micrographs were recorded with a Jeol 1200 EXII
223 electron microscope operating at 100 kV.

224 **Western Blot analysis**

225 Samples used for Western blot analysis were prepared as described previously
226 (23). The antibody used in this study was a rabbit polyclonal serum specific for IBDV VP3
227 (34). After incubation with the primary antibody, membranes were incubated with goat
228 anti-rabbit IgG-Peroxidase conjugate (Sigma-Aldrich). Immunoreactive bands were
229 detected by enhanced chemiluminescence (GE Healthcare).

230 **IFN-β promoter activation assay**

231 DF-1 cells were transfected with 400 or 800 ng of plasmid pIF(-116/+72)lucter
232 (pIFNβ-luc), expressing the *Photinus pyralis* luciferase gene under the control of the
233 human IFN-β promoter (35), along with 30 ng of pRL-null, constitutively expressing the
234 *Renilla muelleri* luciferase gene (Promega Biotech, Spain). The latter used as transfection
235 control. Cells were simultaneously transfected with 400 or 800 ng of pCDNA3 derived
236 plasmids expressing the different VP3 protein versions, or with identical amounts of
237 empty pcDNA3. All samples received the same amount of total DNA, that was adjusted

238 by adding the required amount of pcDNA3. At 8 h post-transfection, IFN-β promoter
239 activity was induced by transfecting 250 ng of poly I:C (average size 0.2-1 kb) (InvivoGen,
240 France) during 16 h. After this period, cell lysates were collected and analysed using the
241 dual-luciferase assay kit (Promega Biotech) following the manufacter's instructions.
242 Luciferase activities were recorded using an Orion II luminometer (Titerthek Berthold,
243 Germany). *Photinus* luciferase activity was expressed as the relative fold induction (n-
244 fold) over that detected in the pcDNA3-transfected cells, after normalization to the
245 *Renilla* luciferase activity.
246

247 **RESULTS**

248 ***In silico* VP3-dsRNA interaction model**

249 As described above, our attempts to solve the crystal structure of the VP3-dsRNA
250 complex have not yet been successful. However, the previously described atomic
251 structure of VP3 (26) together with our preliminary mapping of the VP3 dsRBD (25)
252 prompted us to generate a hypothetical interaction model. Here, we propose an *in silico*
253 model allowing a feasible electrostatic docking of the VP3 protein (pdb: 2r18) and the
254 A-form of the dsRNA helix (pdb: 1RNA). As shown in Fig. 1A, the electronegative side
255 chains of Patch1 residues K99 and K106, located on α-helix 2 of VP3, are spaced by 12.3
256 Å. This distance is rather close to the 13.9 Å gap spacing the OH^- groups from 5'-
257 phosphates of nucleotides n1 and $n9_c$ (the latter corresponding to the complementary
258 RNA strand) within the major groove of the dsRNA helix. This suggests that both
259 phosphates could be efficiently trapped by K99 and K106 residues. In this context, the
260 closely located R126 (VP3 α-helix 1) and the hydrophobic I103 residue (VP3 α-helix 2)
261 could also play a significant role stabilizing the complex, either assisting K99/K106-
262 mediated interactions and/or blocking the displacement of the dsRNA. The Patch2
263 subdomain, placed below Patch1 within the same face of the VP3 monomer, would also
264 contribute to stabilizing dsRNA binding. Both dsRBD subdomains are off centered the
265 vertical VP3 axis, with Patch2 facing the half of α-helix 2 harboring the seemingly crucial
266 Patch1 K99 and K106 residues (Fig. 1B). The average distance between K99 and the
267 clustered electropositive residues forming Patch2 is of 37.3 Å, fairly close to the 37.7 Å
268 gap spacing the OH^- groups from the 5´-phosphates of nucleotides n1 and $n17_c$ at the
269 major dsRNA helix groove.

270 According to the model, stable VP3-dsRNA complex formation would be strictly
271 dependent upon the length of the interacting dsRNA helix providing a suitable platform
272 for the correct positioning of both VP3 dsRBD subdomains. According to the model, a
273 perfectly base-paired dsRNA helix formed by 17-bp should support the engagement of
274 both Patch1 and Patch2 subdomains whilst a shorter one formed by 9-bp would allow a
275 weaker interaction with Patch1.

276 Indeed, these theoretical helix sizes are prone to variations due to the inherent
277 instability of the helix, which is especially high at both ends. This phenomenon, known
278 as "breathing", has been thoroughly described in the DNA helix and reflects
279 spontaneous local conformational fluctuations within double-stranded DNA leading to
280 the breaking of base pairs at temperatures below the melting temperature (36). Indeed,
281 the breathing of dsRNA analytes used in our study might impose some deviation of
282 experimental data with respect to the proposed model.

283 **Kinetic analysis of the VP3-dsRNA interaction**

284 Previous work from our laboratory showed that hVP3, a recombinant version of
285 the VP3 polypeptide harbouring an N-terminal polyhistidine tag, efficiently binds
286 purified IBDV dsRNA genomic segments (ca. 3 Kb) as well as short (21- and 26-bp)
287 synthetic dsRNA duplexes (25). That study was based on the use of electrophoretic
288 mobility assays (EMSA), an experimental approach based on equilibrium analysis that
289 does not provide information about protein-dsRNA binding kinetics. Hence mechanistic
290 details about the VP3-dsRNA interaction remained unknown.

291 Indeed, testing the interaction model described above required a more
292 sophisticated approach allowing to compare the performance of different RNA duplexes
293 and mutant VP3 versions. For this, we resorted to the use of SPR, a highly sensitive

294 approach providing real time quantitative binding kinetics data and allowing the
295 detection of weak protein-dsRNA interactions (37).

296 In order to obtain a comprehensive analysis of the hVP3-dsRNA interaction,
297 biotinylated RNA duplexes of different lengths (10-, 12-, 14-, 16-, 18-, 20-, 22-, 24-, 32-
298 and 40-bp) were captured on the surface of different flow cells of a streptavidin-coated
299 sensor-chip. Analyses were then performed by injecting different concentrations
300 (ranging from 0.313 to 20 nM) of affinity-purified hVP3 onto the RNA duplexes captured
301 on sensor-chips following the protocol described in the Material and Methods section.

302 Results of this analysis are shown in table 1 and supplemental figure 1. Although
303 our model predicts the binding of VP3 dimers to a helix comprising 10-bps, experimental
304 data show that this is not the case, probably reflecting helix end's instability and the
305 consequent reduction of the available dsRNA length.

306 Complex formation was detected with all other tested RNA duplexes (Suppl. Fig.
307 1). As shown in the corresponding sensorgrams, responses during the hVP3 association
308 and dissociation phases are fast and highly dependent on protein concentration.
309 Recoded information was used to calculate kinetics data using a simple 1:1 Langmuir
310 model including a term for mass transport deficiency. Noteworthy, as shown in Suppl.
311 Fig. 1, data gathered with the 40-bp analyte do not fit the 1:1 Langmuir model, hence
312 precluding the calculation of reliable kinetics data. Indeed, this observation strongly
313 suggests that the 40-bp dsRNA provides an interaction surface allowing to
314 simultaneously accommodate more than one VP3 dimer.

315 A comparison of apparent dissociation constant (K_D) values recorded with
316 duplexes ranging from 12- to 32-bp (Fig. 2) indicates that, as predicted by the model, the
317 dsRNA/VP3 binding affinity is largely proportional to duplex length, showing an increase

318 of over 4 $\log_{10} K_D$ units when comparing data recorded with the 12- and 32-bp dsRNA
319 analytes, respectively.

320 **Mutational analysis of the VP3 dsRBD**

321 Fitting our previous EMSA data (25), the proposed model predicts that both
322 dsRBD subdomains are crucial for the establishment of the dsRNA/VP3 interaction. So,
323 we initiate the mutational assessment of the proposed interaction model by analysing
324 the binding capacity of two previously described mutant VP3 polypeptides, hVP3Patch1
325 and hVP3Patch2, using SPR (25). A cartoon showing the electrostatic three-dimensional
326 surface of wild-type, Patch1 and Patch2, hVP3 dimers used for this analysis is shown in
327 Fig. 2A.

328 The 24-bp biotinylated dsRNA was captured on the surface of parallel flow cells
329 of a streptavidin sensor-chip as described above. Affinity purified wild type hVP3,
330 hVP3Patch1 and hVP3Patch2 polypeptides were then injected on different flow cells at
331 a concentration of 200 nM for 120 s followed by injection of protein dilution buffer to
332 analyse protein dissociation. An unmodified flow cell served as a reference surface for
333 these experiments. In view of the low resonance signals detected with both hVP3Patch1
334 and hVP3Patch2 polypeptides, the association phase for these two proteins was
335 extended to 180 s to get a better binding assessment.

336 Fig. 2B shows a set of representative sensorgrams corresponding to assays
337 performed with the three proteins used in these assays. As expected, a sharp interaction
338 signal was detected with the wild-type hVP3 polypeptide. However, signals gathered
339 with hVP3Patch1 and hVP3Patch2 mutants were exceedingly lower, thus conspicuously
340 revealing the harsh detrimental effect of mutations on both Patch1 and Patch2 dsRBD
341 subdomains. Significantly, the obliteration of Patch1 completely arrests dsRNA binding.

342 In contrast, the hVP3Patch2 mutant protein lacking the Patch2 dsRBD subdomain retains
343 a marginal, yet detectable, capacity to interact with the dsRNA analyte. This observation
344 is consistent with the accessory role of the dsRBD Patch2 subdomain predicted by the
345 interaction model described above.

346 Next, to assess the specific contribution of individual Patch1 residues, we
347 generated a set of hVP3 polypeptides holding single amino acid substitutions replacing
348 each electropositive residue (K or R) by an electronegative D residue. The resulting
349 protein mutants (hVP3K99D, hVP3R102D, hVP3K105D and hVP3K106D) were tested
350 using parallel flow cells loaded with the 24-bp RNA duplex. Assays were performed by
351 injecting purified proteins at three concentrations (i.e. 50, 100 and 200 nM) using a 60 s
352 association phase. As shown in Fig. 3A, while hVP3R102D and hVP3K105D retain a dose-
353 dependent binding capacity, this activity is completely abolished in their hVP3K99D and
354 hVP3K106D counterparts.

355 To further confirm data gathered with single point hVP3 mutants, a set of double
356 mutants within the dsRBD Patch1 subdomain (hVP3K99D/R102D, hVP3K99D/K105D,
357 hVP3K99D/K106D, hVP3R102D/K105D, hVP3R102D/K106D and hVP3K105D/K106D)
358 were generated and tested by SPR. The results of this analysis, shown in Fig. 3B, indicate
359 that the dsRNA binding capacity is exclusively retained by the hVP3R102D/K105D
360 mutant protein. Significantly, the only mutant holding unaltered K99 and K106 residues.

361 Taken together this set of results show that, as predicted by the VP3-dsRNA
362 interaction model, both K99 and K106 are absolutely essential for VP3-dsRNA complex
363 formation.

364 **VP3 residues K99 and K106 play a key role counteracting the innate antiviral response**

365 Binding to the viral dsRNA genome represents a key function of VP3 to evade
366 cellular dsRNA sensors that would otherwise trigger the innate antiviral response. In
367 light of the different dsRNA binding activities observed for the tested VP3 mutant
368 versions, it seemed feasible to hypothesize a correlation between the dsRNA-binding
369 affinity and the capacity to control the activation of the innate antiviral response.
370 Accordingly, we compared the capacity of VP3 and its derived mutant versions to
371 hamper the activation of the innate antiviral activity triggered by dsRNA transfection
372 (Fig. 4). For this, we designed an experimental approach allowing to quantify the
373 transcriptional activation of the IFN-β promoter in response to synthetic Poly I:C dsRNA
374 transfection.

375 DF-1 chicken cells were cotransfected with pIFNβ-luc, expressing the *Photinus*
376 *pyralis* luciferase gene (PL) under the control of the IFN-β promoter, and a pcDNA3-
377 derivative constitutively expressing each VP3 version under analysis; pRL-null,
378 constitutively expressing the *Renilla muelleri* (RL) luciferase gene was used as
379 transfection control. 18 h later, cultures were transfected with Poly I:C to trigger the
380 transcriptional activation of the IFN-β promoter. After 16 h, cells were collected and the
381 corresponding extracts used to quantify both PL and PR activities.

382 As shown in Fig. 4, transfection of poly I:C induced a strong activation of the IFN-
383 β promoter in cells transfected with the empty pcDNA3 vector control. This activation is
384 strongly reduced in the presence of wild type VP3, suggesting that the synthetic dsRNA
385 is sheltered by the protein and thus, not detected by cellular sensors. As expected,
386 expression of the VP3Patch1 mutant, unable to bind dsRNA, shows high levels of IFN-β
387 promoter activation, almost as high as those found with the empty vector control; and
388 in the case of the VP3Patch2 mutant, IFN-α activation levels are significantly reduced.

389 Interestingly, when expressing the VP3 versions bearing single amino acid
390 substitutions on the Patch1 dsRBD subdomain we observed that only VP3R102D and
391 VP3K105D were able to reduce IFN-α promoter activation to levels similar to those
392 achieved with the VP3 wild type. VP3K99D and VP3K106D mutants behaved similarly to
393 VP3Patch1, and in both cases poly I:C transfection induced a strong activation of the IFN-
394 β promoter due to the sheltering deficiency of both mutant proteins.

395 In all cases, a VP3 dose-dependent response is observed, further supporting the
396 correlation between the capacity to interact with dsRNA and the evasion from the
397 cellular sensors. Remarkably, the substitution of only one residue, either K99 or K106,
398 completely abolishes the capacity of the protein to evade the antiviral response. Indeed,
399 this finding offers a new and interesting therapeutic target that could be further
400 explored in the future.

401 **VP3 residues K99 and K106 are essential for IBDV replication**

402 In view of results described above it was of outmost importance to determine
403 the effect that K99D and K106D mutations might exert on IBDV replication. For this, we
404 used a previously described reverse genetics approach based on the use of two
405 plasmids, i.e. pT7_SA_Rz and B pT7_SB_Rz, harbouring cDNA sequences corresponding
406 to IBDV genome segments A and B under the transcriptional control of the T7
407 bacteriophage RNA polymerase (32). VP3K99D and VP3K106D substitutions were
408 introduced into the IBDV segment A coding sequence by site-directed mutagenesis. The
409 resulting plasmids pT7_SA-VP3K99D_Rz and pT7_SA-VP3K106D_Rz respectively, were
410 used to cotransfect QM7 cells along with the plasmid pT7_SB_Rz, expressing segment
411 B. As a control for these experiments, cultures were cotransfected with plasmids
412 pT7_SA_Rz and pT7_SB_Rz expressing cDNAs corresponding to wild-type IBDV genome

413 segments A and B, respectively. After transfection, cultures were infected with
414 VT7LacOI, a recombinant vaccinia virus expressing the T7 RNA polymerase upon
415 addition of IPTG to cell media. Cultures were then maintained in the presence of the
416 IPTG to trigger transcription of both IBDV genome segments. At 72 h PI, cell
417 supernatants were harvested and used to detect infectious IBDV by plaque assay.
418 Supernatants were also used to further amplify infectious IBDV by two consecutive
419 rounds of infection on fresh QM7 cell cultures. Results presented in Table 2, indicate
420 that both, VP3K99D and VP3K106D, mutations are lethal, completely abolishing the
421 production of an infective IBDV progeny.

422 Western blotting analysis performed with samples from transfected/infected
423 cultures showed that the mutations under analysis do not affect VP3 expression. This
424 rules out the possibility that the failure to recovering infectious IBDV might be due
425 defects on the expression of mutant VP3 genes (Fig. 5A).

426 The VP3 polypeptide acts as an essential scaffolding element during IBDV particle
427 assembly (9). Accordingly, it seemed feasible that mutations under analysis might alter
428 capsid morphogenesis. Therefore, we next analysed the effect of both VP3K99D and
429 VP3K106D on the assembly of IBDV virus-like particles (VLP). Two recombinant vaccinia
430 viruses VT7_POLY-VP3K99D and VT7_POLY-VP3K106D, expressing mutant versions of
431 the IBDV polyprotein gene, harbouring either the VP3K99D or the VP3K106D point
432 mutations, were generated. The previously described VT7_POLY recombinant vaccinia
433 virus, expressing the wild-type polyprotein gene, known to direct the assembly of IBDV
434 VLP (34), was used as a control for subsequent experiments. These three recombinant
435 viruses were used to infect cultures of BSC-1 cells. Infected cultures were maintained in

436 the presence of the IPTG to trigger the expression of the different polyprotein gene
437 versions.

438 IBDV capsid assembly was tested using two complementary approaches: i)
439 transmission electron microscopy analysis of cells infected with the described
440 recombinant vaccinia viruses; and ii) sucrose gradient-based purification of VLP from
441 infected cell extracts. As shown in Fig. 5B, regardless of the polyprotein gene version
442 being expressed, typical honeycomb-like IBDV-derived VLP superstructures were
443 detected within the cytoplasm of infected cells. Additionally, icosahedral VLPs identical
444 to *bona fide* IBDV particles were isolated from extracts corresponding to cells expressing
445 all three genes under analysis (Fig. 5C). Hence, showing that neither K99D nor K106D
446 affect the VP3 scaffolding activity.

447

448 **DISCUSSION**

449 RNPs are a distinctive structural and functional hallmark differentiating
450 Birnaviruses from prototypical dsRNA viruses deserving an in depth characterization.
451 Indeed, the lack of VP3-dsRNA complex model posed a major obstacle to both
452 understanding mechanisms governing RNP assembly/disassembly processes and to
453 exploring the RNP's contribution to the birnavirus replication process.

454 Here, we present a hypothetical model based on the *in silico* docking of the VP3
455 dimer on the A-form dsRNA helix suggesting that complex formation relies on the
456 establishment of electrostatic interactions between the RNA duplex and VP3 dimers.
457 The first one involving OH^- groups from 5'-phosphates of nucleotides n1 and $n9_c$, within
458 the major dsRNA groove, and electropositive side chains of VP3 residues K99 and K106,
459 located at the Patch1 region. According to the model, a second interaction is established
460 between the OH^- group from 5'-phosphate of $n17_c$, also placed at the RNA's major
461 groove, and electropositive Patch2 residues. In this scenario, the interaction mediated
462 by the dsRBD Patch1 subdomain would play a major role, docking the VP3 dimer on the
463 major groove of the RNA helix, whilst the Patch2 subdomain would have a secondary
464 function stabilizing the complex by further engaging the protein dimer on the major
465 groove of the next helix turn. The model predicts that complex assembly to be strictly
466 dependent on the length of the RNA duplex. So, stable complexes, engaging both VP3
467 Patch1 and 2 regions, would only be formed with dsRNA molecules offering a perfectly
468 base-paired helix comprising at least 17-bp. VP3 dimers should also weakly interact with
469 smaller RNA duplexes holding a flawless helical structure comprising at least 9-bp.

470 The robustness of the proposed model was tested using a SPR-based approach
471 using both a range of dsRNA analytes of different sizes and recombinant VP3
472 polypeptides harbouring mutations on the previously described dsRNA subdomains.
473 Results gathered with the different dsRNA analytes are conclusive showing that,
474 as predicted by the model, VP3/dsRNA complex formation is utterly dependent on
475 dsRNA length. Although predictions concerning helix size requirements are bound to be
476 affected by the inherent dsRNA instability, experimental data roughly fit the proposed
477 model. Hence, showing a clear correlation between the size of the dsRNA analytes and
478 the VP3 binding affinity. The analysis performed with VP3 mutant protein versions
479 confirm the involvement of both dsRBD subdomain, Additionally, as predicted by the
480 model, the analysis show that the electropositive Patch1 subdomain plays a chief role in
481 complex formation. Data collected from the analysis of mutant VP3 polypeptides
482 harbouring Patch1 single and double amino acid substitutions demonstrate that, as
483 predicted by the *in silico* model, residues K99 and K106 are absolutely essential for the
484 interaction to take place. Taking together SPR data presented are in good agreement
485 with the proposed dsRNA/VP3 interaction model.

486 **The role of RNPs on IBDV replication**

487 As described above, experimental data gathered during the assessment of the
488 dsRNA/VP3 interaction model showed the essential role of both VP3 residues K99 and
489 K106. Indeed, the replacement of either one of these residues by an electronegative
490 amino acid completely abrogates the dsRNA binding capacity of the protein. We took
491 advantage of this finding in order to analyse the effect of such mutations on the capacity
492 of the protein to hinder the recognition of dsRNA by cellular dsRNA sensors and the
493 subsequent activation of the innate antiviral response. The results of this analysis

494 conclusively show that both residues are critical to counteracting the dsRNA-triggered
495 innate host's response. Moreover, here we show that although these mutations do not
496 affect the VP3 scaffolding activity, allowing capsid morphogenesis, their introduction
497 within the virus genome completely preclude virus replication. Hence showing for the
498 first time how the introduction of a single amino acid substitution (either K99D or
499 K106D) efficiently abrogates the ability of the virus to complete its replication
500 programme. Certainly, these two critical amino acid residues offer a highly promising
501 target for the design of structure-based of IBDV-specific antivirals. Indeed, data
502 presented here underscore the utmost importance of RNP complexes during the IBDV
503 life cycle.

504 **Insights into the IBDV replication cycle**

505 According to SPR data, VP3-dsRNA association and dissociation phases are fast
506 and highly dependent upon protein concentration. This was somehow expected due to
507 the predicted roles of RNPs during the IBDV replication process; i.e. acting as
508 transcription/replication devices, hindering dsRNA sentinel cellular proteins and likely
509 cooperating to the encapsidation of the virus genome.

510 In order to facilitate the transcription/replication process, VP3 dimers should
511 readily dislodge from dsRNA, thus allowing the synthesis of the nascent RNA daughter
512 chain without affecting the processivity of the viral RdRp. The apparent K_D of VP3 dimer
513 interaction with duplexes ranging from 20- to 24-bp dsRNA is ca. 2 nM. Similar studies
514 conducted with other virus-encoded RNA-interacting proteins rendered kinetic
515 constants comparable to that detected with VP3, e.g. the structural NP protein of
516 Influenza virus (K_D = 8.27 ± 1.43 nM) (38); or the N nucleocapsid protein of coronaviruses
517 (K_D = 0.66-2.82 nM) (39,40). Although experimental differences preclude a direct

518 comparison, our data indicate that the affinity VP3 for dsRNA is not too far off from
519 those recorded with other viral RNA-binding proteins.

520 Additionally, VP3 dimers should swiftly bind the newly synthesized dsRNAs, thus
521 preventing dsRNA detection. Indeed, VP3 dimer binding should be favoured by the high
522 concentration of this protein detected at IBDV replication sites (20).

523 The proposed VP3-dsRNA interaction model suggests that IBDV replication leads
524 to formation of a complex network built by intertwined genome segments, reversibly
525 glued by VP3 dimers within the cell cytoplasm. Such network would act as a molecular
526 trap engulfing newly synthesized RNP components, i.e. dsRNA, VP3 and VP1. This
527 probably explains the presence of rather large viral factories within discrete cytoplasmic
528 areas of IBDV infected cells (41). In addition to conferring an effective shield against
529 specialized host's dsRNA sensors, this RNP network might also serve as a convenient
530 platform to facilitate interactions between pVP2, the capsid precursor polypeptide, and
531 RNP-associated VP3 dimers, probably facilitating the previously described random
532 packaging of genome segments (13) during the IBDV assembly process.

533 According to previously published data, the large majority of infectious IBDV
534 particles package four genome segments in a random manner (13). This accounts for a
535 total RNA duplex length of ca. 12,200-bp per particle (four segments with an average
536 length of 3,050-bp). We have also shown that IBDV virions contain 457±50 VP3
537 monomers (228±25 dimers) (13). Each VP3 dimer possesses two dsRBDs, one at each
538 dimer face, thus being able to simultaneously interact with two dsRNA molecules. Our
539 experimental data indicates that the RNA duplex size stably holding two VP3 dimers is
540 of 20-24-bp. Provided this is maintained under natural infection conditions, a simple
541 calculation, based on available genome and VP3 stoichiometric data, indicates that the

542 number of VP3 dimers required to completely enfold the four dsRNA genome segments
543 found in IBDV particles should be between 305 and 254, quite close to the figure found
544 in purified IBDV virions. This suggests that RNPs released into the cytoplasm from
545 infecting virus particles are fully protected by VP3 dimers. Hence, providing a
546 mechanism to ensuring the stealth of the initial virus replication steps.
547

ACKNOWLEDGEMENTS

We are grateful to the excellent technical assistance provided by Antonio Varas.

FUNDING

This work was supported by the Spanish Ministry of Economy and Competitiveness [AGL2014-60095-P]; Ministry of Science, Innovation and Universities [AGL2017-87464-C2-1-P]; Spanish Ministry of Science and Education [BES-2007-15089 to I.B.] and Spanish Senior Council of Scientific Research [PIE-201420E109 to L.K.]. Work in Barcelona was supported by the Spanish Ministry of Economy and Competitiveness [BIO2017-83906-P] and [MDM-2014-0435].

CONFLICT OF INTEREST

None.

562 **REFERENCES**

563 1. Saunders,L.R. and Barber,G.N. (2003) The dsRNA binding protein family: critical
564 roles, diverse cellular functions. FASEB J., 17(9): 961-83. DOI: 10.1096/fj.02-
565 0958rev
566 2. Wang,X., Vukovic,L., Koh,H.R., Schulten,K. and Myong,S. (2015) Dynamic
567 profiling of double-stranded RNA binding proteins. Nucleic Acids Res., 43(15):
568 7566-76. DOI: 10.1093/nar/gkv726
569 3. Jensen,S. and Thomsen,A.R. (2012) Sensing of RNA Viruses: a Review of Innate
570 Immune Receptors Involved in Recognizing RNA Virus Invasion. J. Virol., 86(6):
571 2900-2910. DOI: 10.1128/JVI.05738-11
572 4. Delmas, D., Attoui, H., Ghosh, S., Malik, Y.S., Mundt, E., Vakharia, V.N., and ICTV
573 Report Consortium, 2019, ICTV Virus Taxonomy Profile: *Birnaviridae*, Journal of
574 General Virology, 100, 5–6. DOI: 10.1099/jgv.0.001185
575 5. van den Berg,T.P., Eterradossi,N., Toquin,D. and Meulemans,G. (2000) Infectious
576 bursal disease (Gumboro disease). Rev Sci Tech., 19: 509-43.
577 6. Kibenge,F.S., Qian,B., Cleghorn,J.R. and Martin,C.K. (1997) Infectious bursal
578 disease virus polyprotein processing does not involve cellular proteases. Arch
579 Virol., 142: 2401-19. DOI: 10.1007/s007050050251
580 7. Sánchez,A.B. and Rodríguez,J.F. (1999) Proteolytic processing in infectious bursal
581 disease virus: identification of the polyprotein cleavage sites by site-directed
582 mutagenesis. Virology., 262: 190-9. DOI: 10.1006/viro.1999.9910
583 8. Maraver,A., Oña,A., Abaitua,F., González,D., Clemente,R., Ruiz-Díaz,J.A.,
584 Castón,J.R., Pazos,F. and Rodríguez,J.F. (2003) The oligomerization domain of
585 VP3, the scaffolding protein of infectious bursal disease virus, plays a critical role
586 in capsid assembly. J Virol., 77(11): 6438-49. DOI: 10.1128/jvi.77.11.6438-
587 6449.2003
588 9. Oña,A., Luque,D., Abaitua,F., Maraver,A., Castón,J.R. and Rodríguez,J.F. (2004)
589 The C-terminal domain of the pVP2 precursor is essential for the interaction
590 between VP2 and VP3, the capsid polypeptides of infectious bursal disease virus.
591 Virology., 322(1): 135-42. DOI: 10.1016/j.virol.2004.01.025

592 10. Saugar,I., Irigoyen,N., Luque,D., Carrascosa,J.L., Rodriguez, J.F. and Castón,J.R.
593 (2010) Electrostatic interactions between capsid and scaffolding proteins
594 mediate the structural polymorphism of a double-stranded RNA virus. J Biol
595 Chem., 285: 3643-3650. DOI: 10.1074/jbc.M109.075994
596 11. Garriga,D., Navarro,A., Querol-Audí,J., Abaitua,F., Rodríguez,J.F. and
597 Verdaguer,N. (2007) Activation mechanism of a noncanonical RNA-dependent
598 RNA polymerase. Proc Natl Acad Sci U S A., 104(51): 20540-5. DOI:
599 10.1073/pnas.0704447104
600 12. Ferrero,D., Garriga,D., Navarro,A., Rodríguez,J.F. and Verdaguer,N. (2015)
601 Infectious Bursal Disease Virus VP3 Upregulates VP1-Mediated RNA-Dependent
602 RNA Replication. J Virol., 89(21): 11165-8. DOI: 10.1128/JVI.00218-15
603 13. Luque,D., Rivas,G., Alfonso,C., Carrascosa,J.L., Rodríguez,J.F. and Castón,J.R.
604 (2009) Infectious bursal disease virus is an icosahedral polyploid dsRNA virus.
605 Proc Natl Acad Sci U S A., 106(7): 2148-2154. DOI: 10.1073/pnas.0808498106
606 14. Lawton,J.A., Zeng,C.Q., Mukherjee,S.K., Cohen,J., Estes,M.K. and Prasad,B.V.
607 (1997) Three-dimensional structural analysis of recombinant rotavirus-like
608 particles with intact and amino-terminal-deleted VP2: implications for the
609 architecture of the VP2 capsid layer. J Virol., 71(10): 7353-7360. DOI:
610 10.1128/JVI.71.10.7353-7360.1997
611 15. Böttcher,B., Kiselev,N.A., Stel'Mashchuk,V.Y., Perevozchikova,N.A., Borisov,A.V.
612 and Crowther,R.A. (1997) Three-dimensional structure of infectious bursal
613 disease virus determined by electron cryomicroscopy. J Virol., 71(1): 325-330.
614 DOI: 10.1128/JVI.71.1.325-330.1997
615 16. Coulibaly,F., Chevalier,C., Gutsche,I., Pous,J., Navaza,J., Bressanelli,S., Delmas,B.
616 and Rey,F.A. (2005) The birnavirus crystal structure reveals structural
617 relationships among icosahedral viruses. Cell. 120(6): 761-72. DOI:
618 10.1016/j.cell.2005.01.009
619 17. Castón,J.R., Rodríguez,J.F. and Carrascosa,J.L. (2008) Infectious Bursal Disease
620 Virus: A Segmented Double-Stranded RNA Virus With a T = 13 Capsid That Lacks
621 a T = 1 Core. In Patton,J.T. (ed.), Segmented Double-Stranded RNA Viruses:
622 Structure and Molecular Biology. Bethesda, USA, Caister Academic Press. DOI:
623 https://doi.org/10.1016/S1473-3099(08)70063-X

624 18. Hjalmarsson,A., Carlemalm,E. and Everitt,E. (1999) Infectious pancreatic necrosis
625 virus: identification of a VP3-containing ribonucleoprotein core structure and
626 evidence for O-linked glycosylation of the capsid protein VP2. J Virol. 73: 3484-
627 90.
628 19. Luque,D., Saugar,I., Rejas,M.T., Carrascosa,J.L., Rodríguez,J.F. and Castón,J.R.
629 (2008). Infectious Bursal disease virus: ribonucleoprotein complexes of a double-
630 stranded RNA virus. J Mol Biol. 386: 891-901. DOI: 10.1128/JVI.73.4.3484-
631 3490.1999
632 20. Dalton,R.M. and Rodríguez,J.F. (2014) Rescue of Infectious birnavirus from
633 recombinant ribonucleoprotein complexes. PLoS One. 9(1):e87790. DOI:
634 10.1371/journal.pone.0087790
635 21. Tan,S.L. and Katze,M.G. (1998) Biochemical and genetic evidence for complex
636 formation between the influenza A virus NS1 protein and the interferon-induced
637 PKR protein kinase. J Interferon Cytokine Res. 18: 757-66. DOI:
638 10.1089/jir.1998.18.757
639 22. Romano,P.R., Zhang,F., Tan,S.L., García-Barrio,M.T., Katze,M.G., Dever,T.E. and
640 Hinnebusch,A.G. (1998) Inhibition of Double-Stranded RNA-Dependent Protein
641 Kinase PKR by Vaccinia Virus E3: Role of Complex Formation and the E3 N-
642 Terminal Domain. Mol Cell Biol. 18: 7304-7316. DOI: 10.1128/mcb.18.12.7304
643 23. Busnadiego,I., Maestre,A.M., Rodríguez,D. and Rodríguez,J.F. (2012) The
644 Infectious Bursal Disease Virus RNA-Binding VP3 Polypeptide Inhibits PKR-
645 Mediated Apoptosis. PLoS One. 7(10):e46768. DOI:
646 10.1371/journal.pone.0046768
647 24. Ye,C., Jia,L., Sun,Y., Hu,B., Wang,L., Lu,X. and Zhou,J. (2014) Inhibition of antiviral
648 innate immunity by birnavirus VP3 protein via blockage of viral double-stranded
649 RNA binding to the host cytoplasmic RNA detector MDA5. J Virol. 88(19): 11154-
650 65. DOI: 10.1128/JVI.01115-14
651 25. Valli,A., Busnadiego,I., Maliogka,V., Ferrero,D., Castón,J.F., Rodríguez,J.F. and
652 García,J.A. (2012) The VP3 Factor from Viruses of Birnaviridae Family Suppresses
653 RNA Silencing by Binding Both Long and Small RNA Duplexes. PLoS One.
654 7(9):e45957. DOI: 10.1371/journal.pone.0045957

655 26. Casañas,A., Navarro,A., Ferrer-Orta,C., González,D., Rodríguez,J.F. and
656 Verdaguer,N. (2008) Structural insights into the multifunctional protein VP3 of
657 birnaviruses. Structure. 16: 29-37. DOI: 10.1016/j.str.2007.10.023
658 27. Ward,G.A., Stover,C.K., Moss,B. and Fuerst,T.R. (1995) Stringent chemical and
659 thermal regulation of recombinant gene expression by vaccinia virus vectors in
660 mammalian cells. Proc Natl Acad Sci U S A. 92(15):6773-7. DOI:
661 10.1073/pnas.92.15.6773
662 28. Méndez,F., de Garay,T., Rodríguez,D. and Rodríguez,J.F. (2015) Infectious bursal
663 disease virus VP5 polypeptide: a phosphoinositide-binding protein required for
664 efficient cell-to-cell virus dissemination. PLoS One. 10(4):e0123470. DOI:
665 10.1371/journal.pone.0123470
666 29. Kochan,G., Gonzalez,D. and Rodríguez,J.F. (2003) Characterization of the RNA-
667 binding activity of VP3, a major structural protein of Infectious bursal disease
668 virus. Arch Virol. 148(4):723-44. DOI: 10.1007/s00705-002-0949-5
669 30. Myszka,D.G. (2000) Kinetic, equilibrium, and thermodynamic analysis of
670 macromolecular interactions with BIACORE. Methods Enzymol. 323: 325-40.
671 DOI: 10.1016/s0076-6879(00)23372-7
672 31. Morton,T.A., Myszka,D.A. and Chaiken,I.M. (1995) Interpreting complex binding
673 kinetics from optical biosensors: a comparison of analysis by linearization, the
674 integrated rate equation, and numerical integration. Anal Biochem. 227(1): 176-
675 85. DOI: 10.1006/abio.1995.1268
676 32. Irigoyen,N., Garriga,D., Navarro,A., Verdaguer,N. Rodríguez,J.F. and Castón,J.R.
677 (2009) Autoproteolytic activity derived from the infectious bursal disease virus
678 capsid protein. J Biol Chem. 284(12):8064-72. DOI: 10.1074/jbc.M808942200
679 33. Rodriguez,J.F., Janeczko,R. and Esteban,M. (1985) Isolation and characterization
680 of neutralizing monoclonal antibodies to vaccinia virus. J Virol. 56(2):482-8. DOI:
681 10.1128/JVI.56.2.482-488.1985
682 34. Fernández-Arias,A., Risco,C., Martínez,S., Albar,J.P. and Rodríguez,J.F. (1998)
683 Expression of ORF A1 of infectious bursal disease virus results in the formation
684 of virus-like particles. J Gen Virol. 79: 1047-54. DOI: 10.1099/0022-1317-79-5-
685 1047

686 35. King P. and Goodbourn S. (1992) A method for sequence-specific deletion
687 mutagenesis. Nucleic Acids Res. 20(5): 1039-1044. DOI: 10.1093/nar/20.5.1039
688 36. Fei J. and Ha T. (2013) Watching DNA breath one molecule at a time. PNAS.
689 110(43): 17173-17174. DOI: 10.1073/pnas.1316493110
690 37. Myszka,D.G. (1997) Kinetic analysis of macromolecular interactions using surface
691 plasmon resonance biosensors. Curr Opin Biotechnol. 8(1):50-7. DOI:
692 10.1016/s0958-1669(97)80157-7
693 38. Liu,C.L., Hung,H.C., Lo,S.C., Chiang,C.H., Chen,I.J., Hsu,J.T.. and Hou,M.H. (2016)
694 Using mutagenesis to explore conserved residues in the RNA-binding groove of
695 infuenza A virus nucleoprotein for antiviral drug development. Sci Rep. 6: 21662.
696 DOI: 10.1038/srep21662
697 39. Chen,H., Gill,A., Dove,B.K., Emmet,S.R., Kemp,C.F., Ritchie,M.A., Dee,M. and
698 Hiscox,J.A. (2005) Mass spectroscopic characterization of the coronavirus
699 infectious bronchitis virus nucleoprotein and elucidation of the role of
700 phosphorylation in RNA binding by using surface plasmon resonance. J Virol.
701 79(2):1164-79. DOI: 10.1128/JVI.79.2.1164-1179.2005
702 40. Spencer,K.A. and Hiscox,J.A. (2006) Characterisation of the RNA binding
703 properties of the coronavirus infectious bronchitis virus nucleocapsid protein
704 amino-terminal region. FEBS Lett. 580(25):5993-8. DOI:
705 10.1016/j.febslet.2006.09.052
706 41. Méndez,F., Romero,N., Cubas,L.L., Delgui,L.R., Rodríguez,D. and Rodríguez,J.F.
707 (2017) Non-Lytic Egression of Infectious Bursal Disease Virus (IBDV) Particles
708 from Infected Cells. PLoS One. 12(1):e0170080. DOI:
709 10.1371/journal.pone.0170080

710 **FIGURE AND TABLE LEGENDS**

711 **Figure 1. In silico VP3-dsRNA interaction model. (A) Matching phosphate distances in**
712 **dsRNA and Patch1 and Patch2 VP3 dsRB subdomains.** The left panel shows a stick
713 representation of a dsRNA structure in a standard A-conformation (PDB id.6BU9). The
714 bases and sugars of each chain are depicted in yellow and green, respectively, with
715 the phosphate groups shown in orange and red for the phosphate and oxygen atoms,
716 respectively. The right panel shows a ribbon representation of IBDV VP3, highlighting
717 the positive residues forming Patch1 and Patch2. The distance between K99 in Patch1
718 and R159 in Patch 2 is 37.3 Å (dashed line), very close to the distance between
719 phosphate groups in a 17 nucleotides dsRNA duplex (labelled in the left
720 panel). The upper central panel shows a close-up of the VP3 Patch1 subdomain. The
721 dashed-line indicates the distance between residues K99 and K106 that is almost
722 coincident with the distance linking the phosphate groups of complementary chains in a
723 9-bp dsRNA region, as shown in the lower central panel. (B) **VP3 dsRBD subdomains.**
724 Left panel, ribbon representation of IBDV VP3 dimer highlighting the electropositive
725 residues forming Patch1 and Patch2, and each VP3 chain in orange and grey,
726 respectively. Central panel, top view of VP3. Right panel, top view of α-helix 1, the
727 dashed line indicates the central part of the secondary structure with most of the
728 electropositive residues facing Patch2**.**

729 **Figure 2. Comparative analysis of the dsRNA binding capacity of Patch1 and Patch2**
730 **hVP3 mutant polypeptides. (A)** hVP3 wt, hVP3Patch1 and hVP3Patch2 protein mutants
731 displayed with its Connolly surface colored according to its electrostatic potential.
732 Residues mutated to alter the electrostatic potential of each hVP3 version are indicated.
733 **(B)** Biacore surface plasmon resonance analysis performed with the wild type (wt),

734 Patch1 (P1) and Patch2 (P2) versions of the hVP3 polypeptide. A biotinylated 24-bp RNA
735 duplex was immobilized on the surface of different cells of a streptavidin sensor-chip.
736 Affinity purified hVP3 protein versions were then injected at 200 nM for 3 min. The
737 graph on the left hand side corresponds to sensograms recorded following the injection
738 of the three proteins under analysis. An enlarged view of sensograms recorded with
739 hVP3Patch1 and hVP3Patch2 polypeptides is presented on the right hand side.

740 **Figure 3. VP3 residues K99 and K106 are necessary for the interaction with dsRNA.**
741 Biacore surface plasmon resonance analysis performed with mutant versions of the
742 hVP3 polypeptide harbouring **(A)** single (hVP3K99D, hVP3R102D, hVP3K105D and
743 hVP3K106D) or **(B)** double (hVP3K99D/R102D, hVP3K99D/K105D, hVP3K99D/K106D,
744 hVP3R102D/K105D, hVP3R102D/K106D and hVP3K105D/K106D) amino acid
745 substitutions on electropositive Patch1 residues. A biotinylated 24-bp RNA duplex was
746 immobilized on the surface of different cells of a streptavidin sensor-chip. Affinity
747 purified hVP3 protein versions were then injected at the indicated concentrations for 1
748 min.

749 **Figure 4. VP3 residues K99 and K106 are essential to counteract the innate antiviral**
750 **response. (A) IFN-α promoter activation.** DF-1 cells were transfected with a plasmid
751 expressing the *Photinus pyralis* luciferase gene under the control of the human IFN-β
752 promoter, along with the pRL-null plasmid, constitutively expressing the *Renilla muelleri*
753 luciferase gene. The latter used as transfection control. Cells were simultaneously
754 transfected with 400 or 800 ng of pCDNA3 derived plasmids expressing the different VP3
755 protein versions, or with identical amounts of empty pcDNA3. At 8 h post-transfection,
756 IFN-β promoter activity was induced by transfecting 250 ng of poly I:C. After 16 h, cell

757 lysates were collected and luciferase activities were recorded. *Photinus* luciferase
758 activity was expressed as the relative fold induction (n-fold) over that detected in the
759 pcDNA3-transfected cells, after normalization to the *Renilla* luciferase activity. Charts
760 correspond to the mean ± the standard deviation of three independent experiments. **(B)**
761 **Expression of VP3 variants.** Western blot analysis (anti-VP3) of the expression of VP3wt
762 and indicated mutants in DF-1 cells.

763 **Figure 5. K99D or K106D mutations do not alter the VP3 scaffolding activity during**
764 **IBDV particle morphogenesis. (A)** Western blot analysis performed with the anti-VP3
765 serum using lysates from QM7 cultures co-transfected with plasmids pT7_SA_Rz and
766 pT7_SB_Rz (WT), pT7_SA-VP3K99D_Rz and pT7_SB_Rz (K99D) and pT7_SA-VP3K106D
767 and pT7_SB_Rz (K106D), respectively, infected with VT7LacOI and maintained either in
768 the presence (+) or absence (-) of IPTG. Untransfected VT7LacOI-infected cells (VT7)
769 were used as control. **(B)** BSC-1 cell monolayers were infected with VT7_POLY (WT),
770 VT7_POLY-VP3K99D (K99D) or VT7_POLY-VP3K106D (K106D), and maintained for 48 h
771 in the presence of IPTG. Cultures were then processed for transmission electron
772 microscopy. Panels show ultra-thin sections corresponding to the cytoplasm of cells
773 infected with the different viruses. Arrows indicate the position of vaccinia virus virions.
774 Scale bars represent 200 nm. **(C)** Electron microscopy images of negatively stained IBDV-
775 like particles purified from BSC-1 cultures infected with VT7_POLY (WT), VT7_POLY-
776 VP3K99D (K99D) or VT7_POLY-VP3K106D (K106D). Scale bars represent 50 nm.

777 **Table 1. Kinetic and affinity constants of the VP3-dsRNA interaction.** Presented data
778 were obtained from sensorgrams shown in supplemental Fig. 1 using the BIAevaluation
779 4.1 software.

780 **Table 2. Reverse genetics analysis of the effect of VP3K99D and VP3K106D mutations**
781 **on the rescue of infectious IBDV.** QM7 cells were transfected with a combination of
782 plasmids pT7-SA-Rz and pT7-SB-Rz, pT7-SAVP3K99D-Rz and pT7-SB-Rz, or pT7-
783 SAVP3K106D-Rz and pT7-SB-Rz, expressing VP3 wild-type, VP3K99D or VP3K106D
784 respectively. At 6 h post-transfection, cultures were infected with 3 PFU/cell of the
785 rVACV VT7. At 72 h PI, supernatants were collected and used to infect fresh QM7 cell
786 monolayers. Samples from these infections were used to perform two subsequent
787 rounds of IBDV amplification by infecting fresh QM7 monolayers. The presence of IBDV
788 was assessed by plaque assay. Presented data corresponds to virus titrations performed
789 in triplicate from samples collected from three independent experiments. (N.D.: not
790 detected).

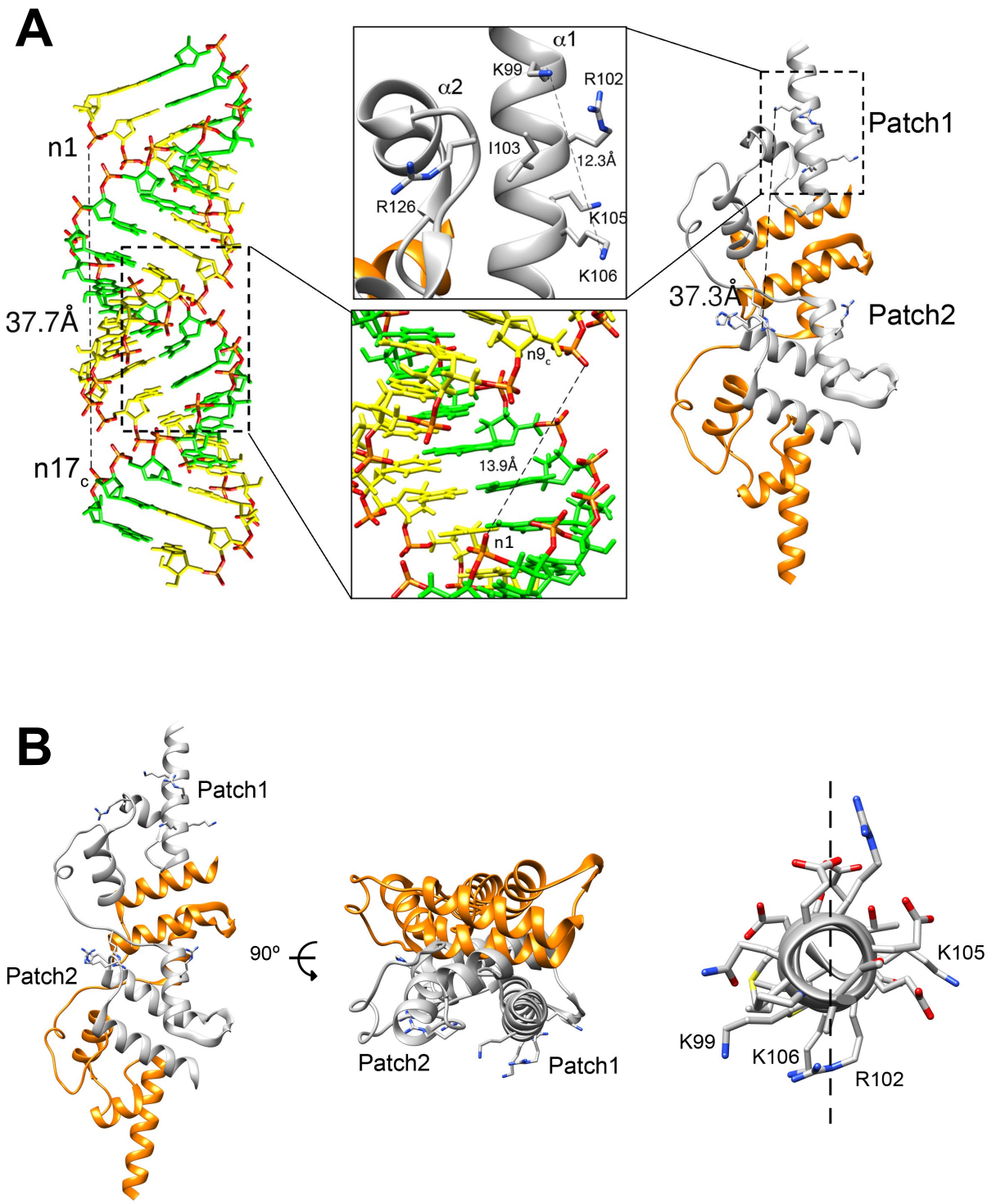
A
n1
37.7Å
n17c
α1
α2
K99
R102
I103
12.3Å
R126
K105
K106
n9c
13.9Å
n1
Patch1
37.3Å
Patch2
B
Patch1
Patch2
90°
Patch2
Patch1
K105
K99
K106
R102

Figure 1

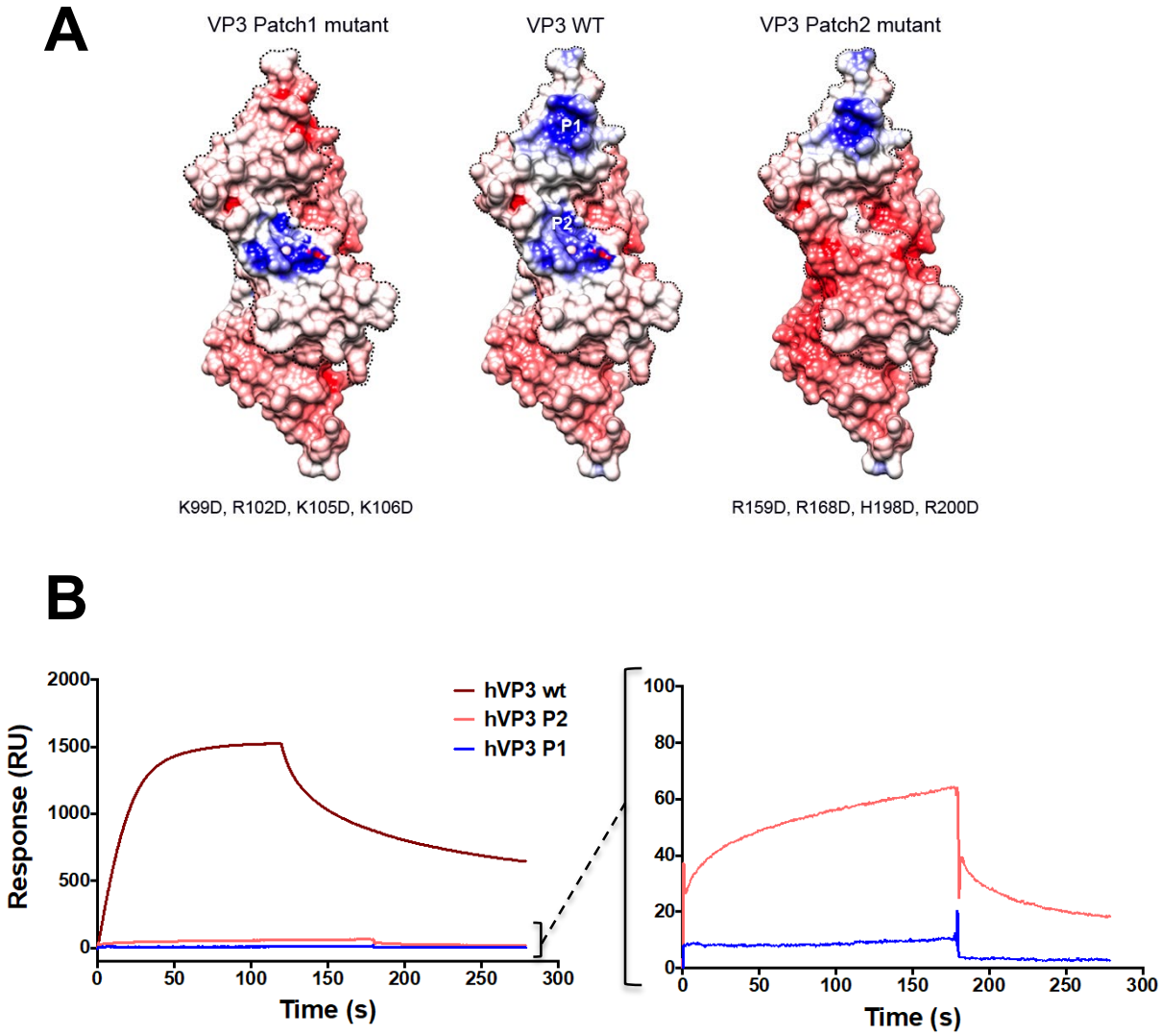
A
VP3 Patch1 mutant
VP3 WT
VP3 Patch2 mutant
P1
P2
K99D, R102D, K105D, K106D
R159D, R168D, H198D, R200D
B
hVP3 wt
hVP3 P2
hVP3 P1
Response (RU)
Time (s)
Time (s)

Figure 2

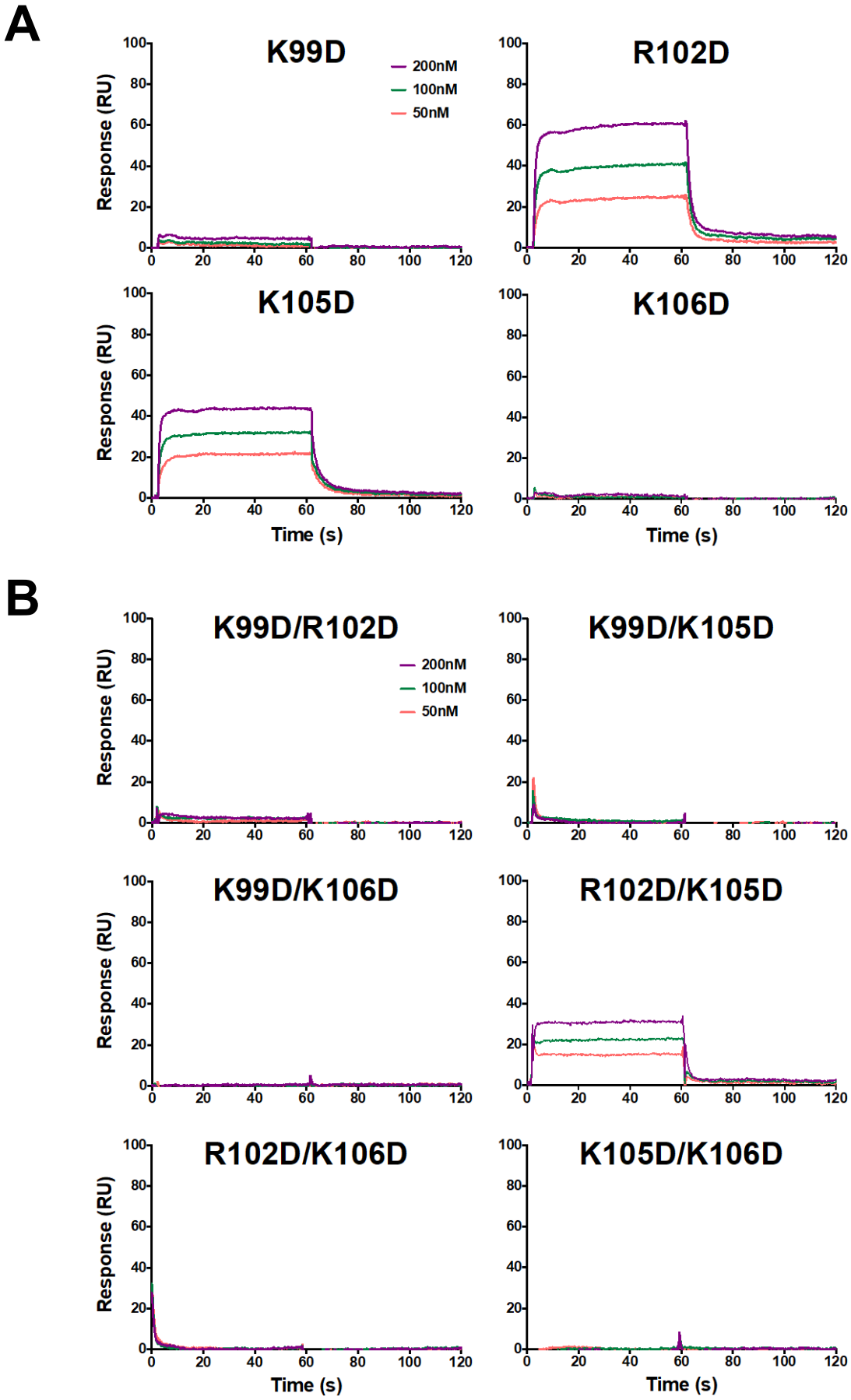
A
K99D
R102D
K105D
K106D
200nM
100nM
50nM
Response (RU)
Time (s)
B
K99D/R102D
K99D/K105D
K99D/K106D
R102D/K105D
R102D/K106D
K105D/K106D
200nM
100nM
50nM
Response (RU)
Time (s)

Figure 3

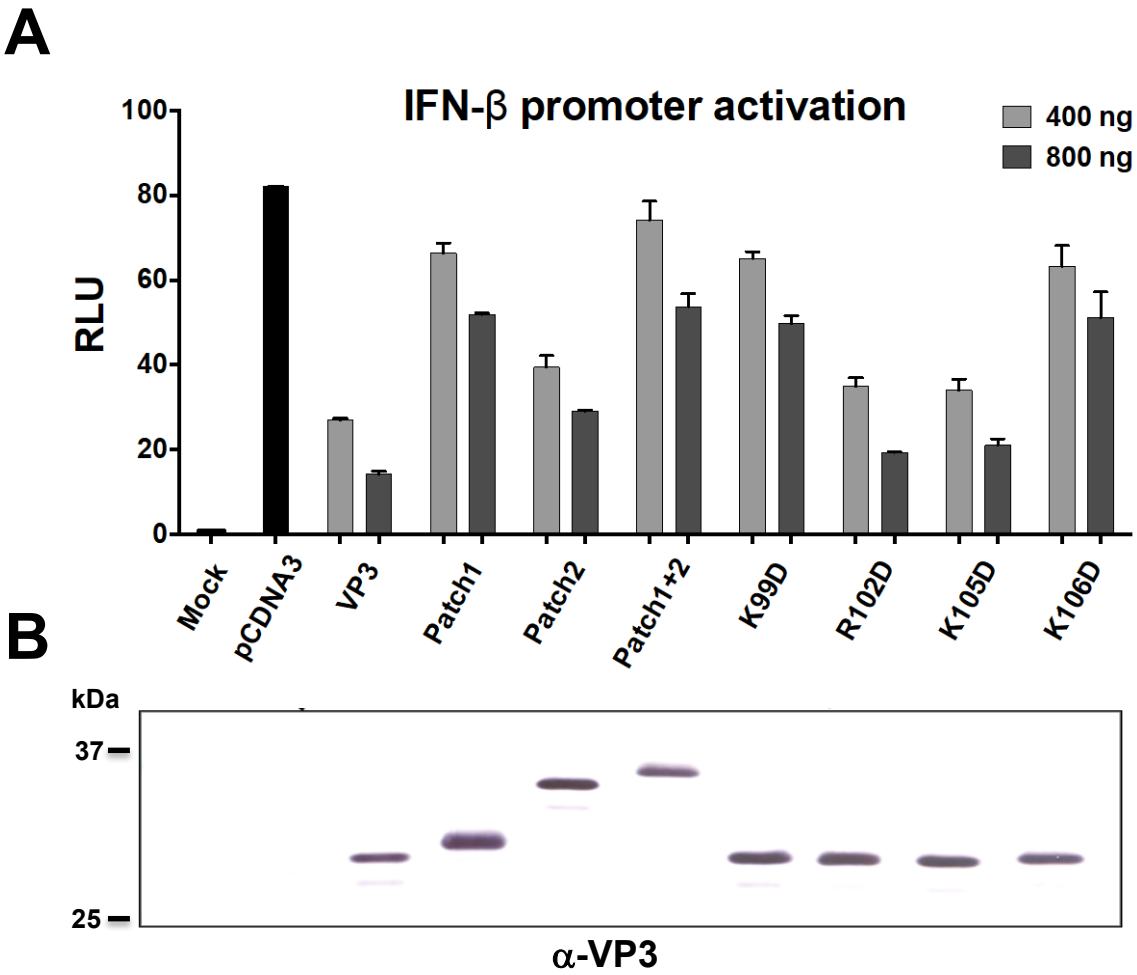
A
IFN-β promoter activation
400 ng
800 ng
RLU
100
80
60
40
20
0
Mock
pCDNA3
VP3
Patch1
Patch2
Patch1+2
K99D
R102D
K105D
K106D
B
kDa
37
25
α-VP3

Figure 4

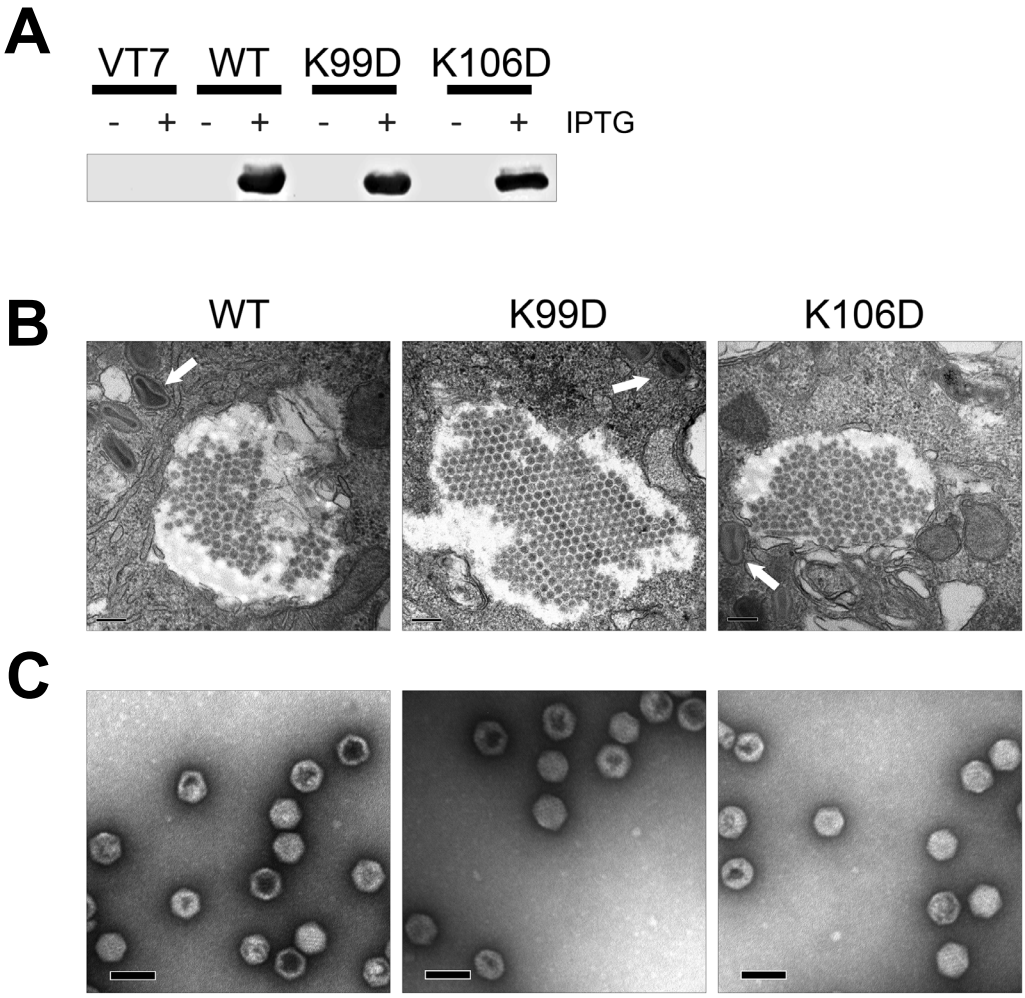

Figure 5

dsRNA length (bp)	k_a ($M^{-1}s^{-1}$)	k_d (s^{-1})	K_D (M)
10	n.d.	n.d.	n.d.
12	1.15×10^{6}	1.76×10^{-1}	1.52×10^{-7}
14	1.11×10^{6}	4.48×10^{-2}	4.05×10^{-8}
16	1.51×10^{6}	4.50×10^{-2}	3.05×10^{-8}
18	3.61×10^{6}	4.41×10^{-2}	1.22×10^{-8}
20	6.26×10^{6}	1.32×10^{-2}	2.12×10^{-9}
22	9.40×10^{6}	3.02×10^{-2}	3.21×10^{-9}
24	7.14×10^{6}	1.42×10^{-2}	2.00×10^{-9}
32	7.73×10^{6}	3.60×10^{-3}	3.99×10^{-10}
40	n.d.	n.d.	n.d.

Table 1. Kinetic and affinity constants of the VP3-dsRNA interaction. n.d. : Not detected.

Table 1

VP3 gene	Virus titers (PFU/ml)		
	First round	Second round	Third round
Wild-type	$2.1 \pm 1.2 \times 10^{2}$	$3.4 \pm 2.3 \times 10^{4}$	$6 \pm 3.1 \times 10^{7}$
VP3K99D	N.D.	N.D.	N.D.
VP3K106D	N.D.	N.D.	N.D.

Table 2. Reverse genetics analysis of the effect of mutations VP3K99D and VP3K106D on the rescue of infectious IBDV.

Table 2